

Energy-based Modelling of the Feedback Control of Biomolecular Systems with Cyclic Flow Modulation

Peter J. Gawthrop^{*1,2}

¹ Systems Biology Laboratory, Department of Biomedical Engineering, Melbourne School of Engineering, University of Melbourne, Victoria 3010, Australia.

²Systems Biology Laboratory, School of Mathematics and Statistics, University of Melbourne University of Melbourne, Victoria 3010

January 29, 2021

Abstract

Energy-based modelling brings engineering insight to the understanding of biomolecular systems. It is shown how well-established control engineering concepts, such as loop-gain, arise from energy feedback loops and are therefore amenable to control engineering insight. In particular, a novel method is introduced to allow the transfer function based approach of classical linear control to be utilised in the analysis of feedback systems modelled by network thermodynamics and thus amalgamate energy-based modelling with control systems analysis. The approach is illustrated using a class of metabolic cycles with activation and inhibition leading the concept of Cyclic Flow Modulation.

Contents

| | | |
|----------|--|-----------|
| 1 | Introduction | 2 |
| 1.1 | Bond graph based modelling of reaction systems | 3 |
| 2 | Bond graph based control analysis | 5 |
| 2.1 | Linearisation | 8 |
| 2.2 | Example: Enzyme-catalysed reaction control | 8 |
| 2.3 | Open-loop analysis | 9 |
| 2.4 | Split Loop analysis | 11 |
| 3 | Cyclic flow modulation (CFM) | 14 |
| 3.1 | Integral action | 17 |
| 3.2 | Steady-state values | 20 |
| 4 | Conclusion | 20 |
| 5 | Acknowledgements | 21 |

*Corresponding author. peter.gawthrop@unimelb.edu.au

1 Introduction

The bond graph implementation of Network Thermodynamics was introduced some 50 years ago as an energy-based approach to modelling biomolecular systems [1, 2]. “Graphical representations similar to engineering circuit diagrams can be constructed for thermodynamic systems. ... such diagrams do increase one’s intuition about system behaviour.”[3].

The design of linear feedback circuits also has a long history and the correspondingly well-established theory of control systems [4] has been applied to biomolecular systems [5–7] and has led to a number of control concepts such as feedback and integral action being used in the biomolecular context [8–11].

Classical linear control theory is based on *transfer function* models of dynamical systems. In contrast, the energy-based approach of this paper uses the bond graph paradigm for modelling biomolecular systems. There has been limited work on the bond graph approach to control [12–14] For this reason, a novel method is introduced to allow the transfer function based approach of classical linear control to be utilised in the analysis of feedback systems modelled by bond graphs and thus combine energy-based modelling with control systems analysis. This approach can, in principle, be used in two distinct ways: to *analyse* existing biomolecular control systems arising from evolution and to *synthesise* new biomolecular control systems for synthetic biology.

As discussed by Gawthrop and Crampin [15], the bond graph approach gives the set of *nonlinear* ordinary differential equations describing the biomolecular system being modelled. Linearisation of non-linear systems is a standard technique in control engineering. Linearisation in the context of bond graph models of biomolecular systems was introduced by Gawthrop and Crampin [15] and is used here.

The role of metabolic cycles in the regulation of metabolic flux is well established [16–18, 9, 19]. Such cycles¹ are involved in a number of substrate conversions including those between fructose-6-phosphate and fructose-1,6-biphosphate, fructose-6-phosphate and fructose-2,6-biphosphate, triglyceride/fatty acid, glucose and glucose-6-phosphate, and glycogen and glucose 1-phosphate [16, 18, 19]. To illustrate the fusion of network thermodynamics and control theory, this paper will focus on the first two inter-conversions involving fructose-6-phosphate (F₆P). Because of the cyclic nature of these two reactions, and the fact that flow is modulated, the term *Cyclic Flow Modulation* (CFM) is used to describe such reaction systems.

The use of CFM requires energy and there is a trade-off between quality of control and energy consumed [17]. It is therefore important to account for energy flows when modelling biomolecular systems and this is done here using the fusion of the network thermodynamics paradigm, as implemented using bond graphs, with control theory. Criteria for robust biochemical reaction networks have been established which ensure zero steady-state error [20–22]; but these papers make no mention of energy and therefore entirely ignore thermodynamic constraints.

Building complex systems is simplified using modularity [23]; but it is essential to distinguish two different concepts of modularity: *computational* modularity where physical correctness is retained and *behavioural* modularity where module behaviour (such as ultra-sensitivity) is retained [15]. As well as providing computational modularity, bond graphs provide a natural formulation of behavioural modularity and reveal the sources of retroactivity [15]. *Chemostats* [15, 24] are used to create an open system from a closed system and also provide a convenient way of providing *ports* to connect bond graph modules.

§ 1.1 provides a brief tutorial introduction to the bond graph approach in this context. § 2 intro-

¹The pejorative term “futile cycle” is often used to describe such cycles; this will be avoided in this paper.

duces the bond graph based approach to the analysis of feedback control systems using an enzyme catalysed reaction with competitive inhibition as an illustrative example. § 3 shows how cyclic flow modulation (CFM) can be used to build effective feedback controllers with approximate integral action. § 4 concludes the paper and gives directions for future work.

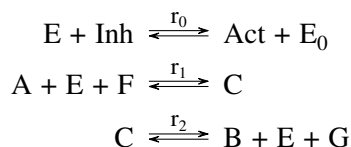
1.1 Bond graph based modelling of reaction systems

A network thermodynamics approach to modelling systems of biochemical reactions was introduced by Oster et al. [1, 2] and utilised the bond graph approach of Paynter [27]. Tutorial introductions to bond graphs are available for control engineers [28] and systems biologists [29]. This section gives a brief introduction to bond graphs focused on the applications in this paper.

Bond graphs focus on the energetic connection between components and the \rightarrow symbol indicates such an energetic connection; the half-arrow indicates the direction corresponding to positive energy flow. In the biomolecular context, each such bond is associated with two covariables: chemical potential μ (J mol^{-1}) and flow v (mol s^{-1}). The key point is that the product of μ and v is power $p = \mu v$ (W). Alternatively, it is possible to scale these co-variable by Faraday's constant F (C mol^{-1}) to give $\phi = \frac{1}{F}\mu$ (V) and $f = Fv$ (A) where (J C^{-1}) has been replaced by the more convenient unit volt (V) and (C s^{-1}) has been replaced by the more convenient unit ampere (A) [26].

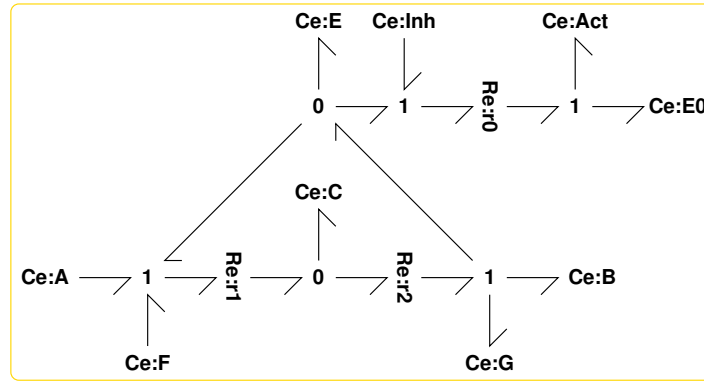
Electrical components may be connected in *parallel* (where the *voltage* is common) and *series* (where the *current* is common). These two concepts are generalised in the bond graph notation as the **0** junction which implies that all impinging bonds have the same *potential* (but different flows) and the **1** junction which implies that all impinging bonds have the same *flow* (but different potentials). The direction of positive energy transmission is determined by the bond half arrow. As all bonds impinging on a **0** junction have the same *potential*, the half arrow implies the sign of the *flows* for each impinging bond. The reverse is true for **1** junctions, where the half arrow implies the signs of the *potentials*.

In this context, *species* are represented **Ce** components and *reactions* by **Re** components. In particular, consider the three reactions

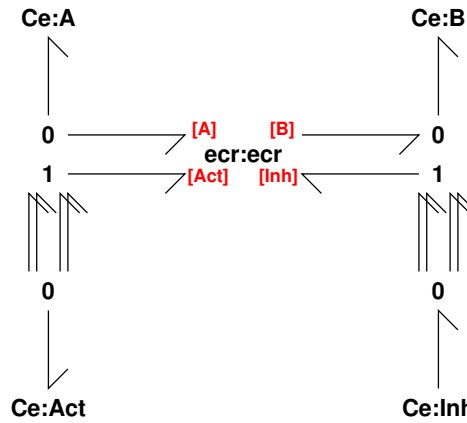


which are represented by the bond graph of Figure 1(a). The species A, B, C etc. are represented by the components **Ce:A**, **Ce:B**, **Ce:C** etc.; the reactions r_1 , r_2 and r_3 are represented by the components **Re:r1**, **Re:r2** and **Re:r3**. Thus, for example, the lower left **1** junction ensures that the flow from the species A, E and F is identical to that though the reaction r_1 . Energy conservation at the junction then implies that the net potential impinging on the left of reaction r_1 is the sum of the species potentials. Similarly, the lower centre **0** junction ensures that the potential of species C appears at the right of reaction r_1 and the left of reaction r_2 . Energy conservation at the junction then implies that the flow into species C is the difference of the flows though reactions r_1 and r_2 .

Figure 1(a) clearly shows the structure of the reaction network in terms of which species are connected to which reactions. As discussed in the caption, Figure 1(b) contains the module **ecr:ecr** containing the bond graph of Figure 1(a); and the four components **Ce:A**, **Ce:B**, **Ce:Act** & **Ce:Inh** are exposed as ports. Thus in Figure 1(b), the arrangement of four bonds collecting **0** and **1** junctions



(a) Enzyme-catalysed reaction (module **ecr**)



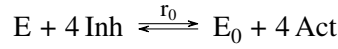
(b) Cooperativity (module **ECR**)



(c) Pathway (module **PATH**)

Figure 1: Enzyme-catalysed reaction (ECR). The Bond Graph notation is: \rightarrow energy connection; **Ce** species; **Re** reaction; **0** common potential connection; **1** common flow connection [25]. Modules containing a bond graph and/or sub-modules are indicated by the notation **module:instance** [15, 26]; thus in (b) **ecr:ecr** represents an instance called “ecr” of the module “ecr” containing the bond graph of (a). Module *ports* are denoted by []; thus port [A] of **ecr** corresponds to the component **Ce:A** of (a). (a) Enzyme-catalysed reaction with competitive activation and inhibition. **Ce:A**, **Ce:B**, **Ce:E**, **Ce:C**, **Ce:Act** & **Ce:Inh** represent the substrate, product, enzyme, enzyme-substrate complex, activation and inhibition respectively. In the sequel, the generic species such as A will be replaced by specific species. **Ce:F** & **Ce:G**, provide the driving energy. Example species appear in Figure 7. (b) A simple model of cooperativity is included by specifying that 4 activation and 4 inhibition species interact with the enzyme; this is achieved in a modular fashion by incorporating the bond graph of (a) into module **ecr**. (c) The module **SYS** (the controlled system) of Figure 2(b) is, in this example, a simple path of 3 reactions represented by **Re:r1–R:r3** with intermediate species **Ce:I1** and **Ce:I2**.

changes the stoichiometry of the first reaction to:



For the purposes of this paper (see [25] for more detail), the mass-action kinetics of the reaction system corresponding to a bond graph representation is obtained from the **Ce** constitutive relation:

$$\phi_A = RT \ln K_A x_A \quad (1)$$

where ϕ_A and x_A are the chemical potential (J mol^{-1}) and concentration relative to standard conditions (dimensionless) of the generic species A, K_A is a dimensionless constant [30, § 1.2] and RT (J mol^{-1}) is the product of the universal gas constant R and absolute temperature T ; the **Re:ri** constitutive relation for the i th reaction

$$v_i = \kappa_i \left[\exp \frac{\Phi^f}{RT} - \exp \frac{\Phi^r}{RT} \right] \quad (2)$$

where v_i is the ratio of the i th reaction flow to a nominal flow (dimensionless), κ_i (dimensionless) is the reaction constant. Φ^f and Φ^r (J mol^{-1}) are the forward and reverse reaction affinities of the i th reaction determined by the species potentials ϕ and the structure of bonds and junctions determining the stoichiometry of the reaction networks. Different forms of the **Re:ri** constitutive relation (2) give rise to different forms of kinetics [31].

Systems of chemical reactions written in terms of rate constants, and the corresponding ODEs are not necessarily consistent with physical principles [30, § 1.3]. In contrast, chemical reactions written as bond graphs automatically obey the Wegscheider conditions [32]. Thus reaction systems modelled in bond graph form can be combined in a modular way [15]; the resultant modular bond graph can then be used to generate an energetically consistent set of ODEs suitable for simulation. Similarly, bond graphs account for the phenomenon of *retroactivity* [7] in a transparent fashion [15].

2 Bond graph based control analysis

Figure 2(a) depicts a conventional feedback control system in transfer-function form. The four transfer functions $G_{con}(s)$, $G_{sys}(s)$, $G_w(s)$ and $G_d(s)$ represent the controller, the system under control, the setpoint and disturbance transfer functions respectively where s is the Laplace variable. The four signals y , u , w and d represent the system output, system input, setpoint and disturbance respectively. In this context, y could be a product whose concentration is to be controlled, u a reaction flow, w the ideal product concentration and d the concentration of another species.

The closed-loop transfer function is:

$$y = \frac{L(s)}{1 + L(s)} G_w(s) w + \frac{1}{1 + L(s)} G_d(s) d \quad (3)$$

$$\text{where } L(s) = G_{con}(s) G_{sys}(s) \quad (4)$$

$L(s)$ is referred to as the *feedback loop gain*. In the engineering context, $G_{con}(s)$ and $G_{sys}(s)$ would arise from separate physical entities; nevertheless, the loop gain $L(s)$ (4) appearing in equation (3) only requires the *product* of $G_{con}(s)$ and $G_{sys}(s)$. This is important for biomolecular systems where there is no clear physical distinction between controller and system: it is the feedback loop itself that is of fundamental importance.

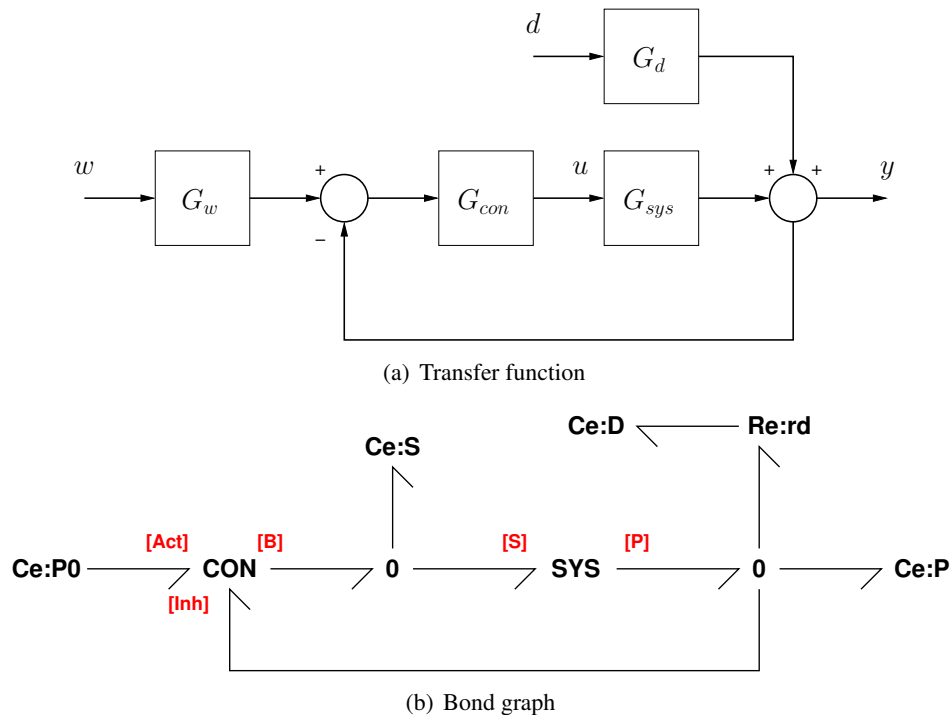


Figure 2: Feedback control. (a) A classical feedback loop block diagram representing the linearisation of a non-linear system. The blocks represent transfer functions which are connected by signals. y is the controlled output, d a disturbance and w the setpoint, or desired value of y . (b) A bond graph feedback loop. **CON** and **SYS** are bond graph *modules* with *ports* denoted by []. The module **CON** will be replaced by various modules in the sequel. In particular, module **ECR** of Figure 1(b) is used as **CON** with three components exposed; the hidden component **Ce:A** is a chemostat in the sequel. **Ce:P**, **Ce:D** and **Ce:P0** are bond graph components representing species corresponding to product, disturbance and reference species respectively. Throughout this paper, the **SYS** component is the pathway system **Path** of Figure 1(c). The \rightarrow symbol indicates an energetic connection between two subsystems; the half-arrow indicates the direction corresponding to positive energy flow. The relationship between the block diagram of (a) and the bond graph of (b) is examined in § 2.3.

Typically, such control systems are analysed in the frequency domain by setting $s = j\omega$ where $j = \sqrt{-1}$ and ω is frequency in rad/sec. At those frequencies where $L(j\omega)$ is large, equation (3) can be approximated by $y \approx G_w(s)w$. In other words, a large loop gain $L(j\omega)$ is desirable insofar as the system output y is a close match to the desired value $G_w(s)w$ despite disturbances represented by d . However, incorrect choice of the the loop gain $L(s)$ can lead to instability and $L(s)$ is, moreover, subject to fundamental constraints [4].

To summarise, there are two potentially conflicting issues in controller design: good disturbance rejection and stability; these are both captured in the loop gain $L(s)$.

Figure 2(a) implicitly assumes that the connection between subsystems, such as those represented by $G_{con}(s)$ and $G_{sys}(s)$ is one-way as indicated by the arrows. However, the physical controller needs to be designed to make sure this one-way interaction is correct; this requires the use of energy. It has been argued that this approach is misguided, even in the context of engineering systems. This has led to the concept of physical-model based control [12–14]

In the context of biomolecular systems, the concept of *retroactivity* [7] has been introduced to explain why interaction is not one-way and thus design based on simplistic application of the approach of Figure 2(a) often fails.

There are two reasons why the bond graph approach is superior to the block diagram approach of Figure 2(a) in the context of feedback control:

1. It explicitly accounts for the two-way interaction found in physical systems in general and biomolecular systems in particular.
2. It explicitly accounts for energy flows and thus can directly expose performance/energy consumption trade-offs; this is the subject of current research.

For this reason, the transfer function paradigm of Figure 2(a) is replaced by the bond graph based paradigm of Figure 2(b).

Figure 2(b) is based on the notation for modular bond graphs [32]. The two bond graph modules are **CON** and **SYS**; **CON** represents the controller and has three ports: [Act] (activation), [Inh] (inhibition) and [Con] (control signal) and **SYS** represents the system and has two ports: [S] (substrate) and [P] product. In the sequel, the system module **SYS** is the pathway **Path** module of Figure 1(c) but the controller module will be instantiated by three modules in turn: an enzyme catalysed reaction with competitive activation and inhibition (§ 2.2), cyclic flow modulation (§ 3) and cyclic flow modulation with integral action (§ 3.1).

The components **Ce:P** and **Ce:S** represent the product and substrate species respectively and the components **Ce:P0** and **Ce:D** represent the reference species and product disturbance respectively; because **Ce:P0** and **Ce:D** represent exogenous variables, they are *chemostats* [24, 15].

Because the paper combines approaches from three fields – systems biology, bond graphs and control theory – there are three notational systems. To summarise, a generic species A has a bond graph representation **Ce:A** and the corresponding “signal” is the concentration x_A . In a particular case, the generic species A can be instantiated as a particular species such as fructose-6-phosphate (**F₆P**).

As shown in the sequel, the bond graph modelling approach can make use of the transfer function approach to understand the dynamic properties of feedback systems of the form of Figure 2(b). In particular, as shown in § 2.3, the fundamental control systems concept of loop-gain can be retrieved from the bond graph modelling paradigm. But first, linearisation must be considered.

2.1 Linearisation

Biomolecular systems are nonlinear and must be linearised before applying transfer function techniques. Linearisation of biomolecular systems in a biomolecular context, together with a discussion on retroactivity, is given by [15]. In particular, the non-linear system equations are:

$$\frac{d}{dt}x = Nf \qquad f = F(x, x_{ch}) \qquad (5)$$

In systems biology terms: the n_x vector x represents the amount of each non-chemostatted species (mol), the $n_x \times n_f$ matrix N is the system *stoichiometric matrix*, the n_f vector f represents the flow in each reaction (mols^{-1}). The $n_{x_{ch}}$ vector x_{ch} represents the amount of each chemostatted species (mol). $F(x, x_{ch})$ is a *nonlinear* function of both arguments. Because of thermodynamic constraints, F has a particular structure dependent on the stoichiometric matrix N [33] and is automatically generated from the bond graph representation. In standard control system terms, x is the system *state*, f is the system *output* and x_{ch} the system *input*.

The corresponding linearised equations are:

$$\frac{d}{dt}\tilde{x} = N\tilde{f} \qquad (6)$$

$$\tilde{f} = C\tilde{x} + D\tilde{x}_{ch} \qquad (7)$$

$$\text{where } \tilde{x} = x - \bar{x} \qquad (8)$$

$$\tilde{x}_{ch} = x_{ch} - \bar{x}_{ch} \qquad (9)$$

$$\tilde{f} = f - \bar{f} \qquad (10)$$

where the $n_f \times n_x$ matrix C and the $n_f \times n_{x_{ch}}$ matrix D are given by the partial derivatives:

$$C = \frac{\partial f}{\partial x} \qquad D = \frac{\partial f}{\partial x_{ch}} \qquad (11)$$

evaluated at the steady-state values \bar{x} and \bar{f} of state and flow respectively corresponding to the constant chemostat state $x_{ch} = \bar{x}_{ch}$:

$$N\bar{f} = 0 \qquad \bar{f} = F(\bar{x}, \bar{x}_{ch}) \qquad (12)$$

Linearisation has two steps: finding the steady-state state \bar{x} and flow \bar{f} and then computing the linearisation matrices C and D . The first is simply accomplished by numerically simulating the system until a steady-state is reached ($\frac{d}{dt}x \approx 0$). The second is achieved symbolically within `BondGraphTools` (<https://pypi.org/project/BondGraphTools>) using the symbolic derivative functions of the `sympy` library (<https://www.sympy.org>). The `Python Control Systems Library` (<https://pypi.org/project/control/>) is used to convert the linearised system from state-space form to transfer function form, manipulate transfer functions and to generate time and frequency responses.

2.2 Example: Enzyme-catalysed reaction control

The modified enzyme-catalysed reaction module of Figure 1(b) and the pathway module of Figure 1(c) are embedded in the feedback loop of Figure 2(b) as **CON** and **SYS** respectively and used for the purposes of illustration; the parameters are given in Figure 3.

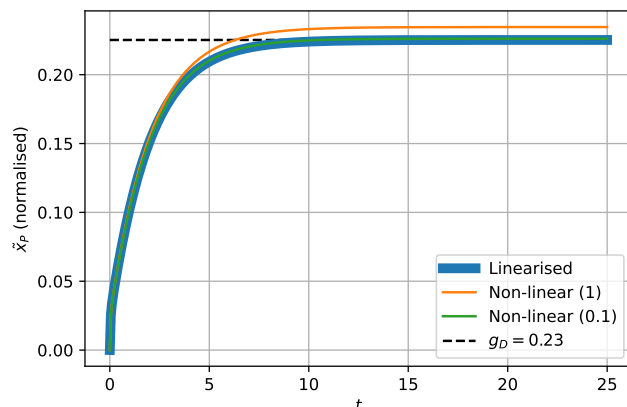


Figure 3: Non-linear and linearised closed-loop step response. The asymptotic value g_D is indicated by a dashed line. The amplitude of the disturbance step is given for the non-linear simulations and the resultant response is divided by the step amplitude. The normalised nonlinear response is close to the linear case for an amplitude of 0.1 and differs slightly for an amplitude of 1.0. For the purposes of illustration, all parameters (which are dimensionless - see § 1.1) are unity except for the species constants for F and G: $K_F = 10^3, K_G = 10^{-3}$ and reaction constants for the controller (Fig. 1(a)): $\kappa_{r1} = \kappa_{r2} = 2$ and system (Fig. 1(c)): $\kappa_{r1} = \kappa_{r2} = \kappa_{r3} = 10$. The steady-state values (which are also dimensionless - see § 1.1) were $x_S = 12.85$ and $x_P = 10.12$.

The non-linear system equations were derived from the modular bond graph of Figure 2(b) using `BondGraphTools` and simulated to give the steady-state condition corresponding to the parameters of Figure 3. The linearised equations were then extracted and the transfer function relating the disturbance \tilde{x}_D to the product \tilde{x}_P generated. The corresponding closed-loop step response appears in Figure 3.

However, simulation does not provide an explanation of why the steady-state is the particular value shown nor why the dynamics are as shown. The explanation is provided by the analysis of the following section.

2.3 Open-loop analysis

As discussed above, the loop-gain $L(s)$ is a key transfer function in the classical control systems analysis of Figure 2(a). This section indicates how the loop-gain $L(s)$ can be derived from the bond graph of Figure 2(b).

The closed-loop system of Figure 2(b) includes two chemostats **Ce:P0** and **Ce:D** which make the corresponding states x_{P0} and x_D independent variables; the product state x_P remains a dependent variable which evolves with time as in Figure 3. To create an open loop system, the component **Ce:P** representing the product is also made a chemostat thus making x_P an independent variable.

The linearised flow \tilde{f}_P into the chemostat **Ce:P** is given by the sum of three terms corresponding to the three chemostats **Ce:P**, **Ce:P0** and **Ce:D** respectively:

$$\tilde{f}_P = -G_P(s)\tilde{x}_P + G_{P0}(s)\tilde{x}_{P0} + G_D(s)\tilde{x}_D \quad (13)$$

where $-G_P, G_{P0}$ and G_D are the transfer functions relating \tilde{f}_P to $\tilde{x}_P, \tilde{x}_{P0}$ and \tilde{x}_D respectively. The

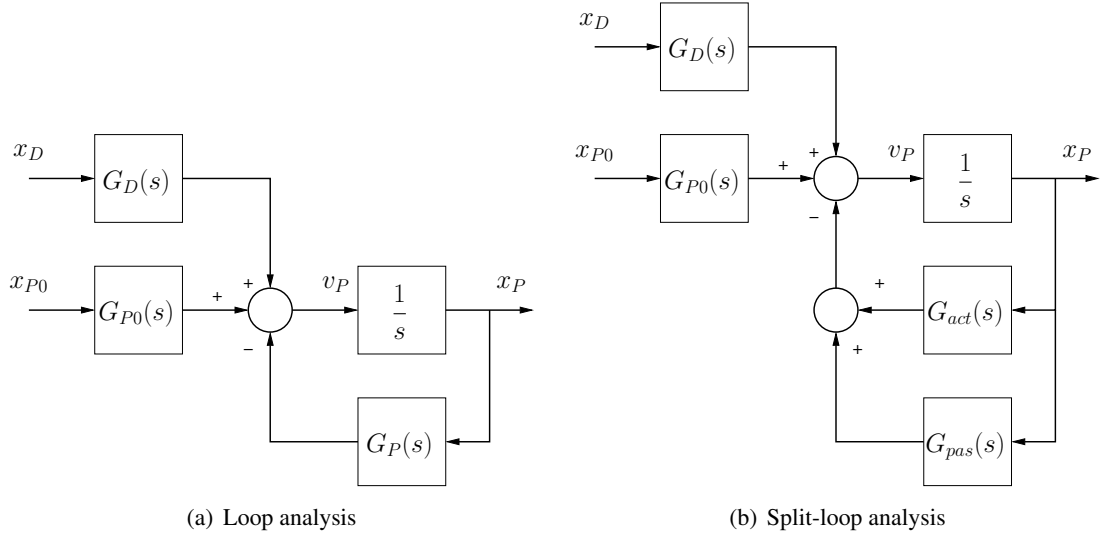


Figure 4: Loop analysis. (a) The block diagram corresponding to opening the bond graph feedback loop by setting the product **Ce:P** to be a chemostat. x_P is the amount of product and v_P the product flow. $G_P(s)$, $G_D(s)$ and $G_{pP0}(s)$ are transfer functions relating x_P , x_D and x_{P0} to f_P . (b) The transfer function $G_P(s)$ is split into two terms: $G_{act}(s)$ and $G_{pas}(s)$ corresponding to active and passive feedback.

minus sign associated with G_P is to give compatibility with standard definitions of loop gain in a negative feedback context.

To reclose the loop, **Ce:P** is restored to non-chemostatted dynamics using the transfer function relating \tilde{x}_P to \tilde{f}_P :

$$\tilde{x}_P = \frac{1}{s} \tilde{f}_P \quad (14)$$

The block diagram corresponding to Equations (13) and (14) is shown in Figure 4(a). Using Equation (4), the loop gain $L(s)$ is given by:

$$L(s) = \frac{G_P(s)}{s} \quad (15)$$

From the block diagram of Figure 4(a), or from Equations (13) and (14), the closed-loop system can be explicitly written as

$$\tilde{x}_P = \frac{1}{s + G_P(s)} [G_{P0}(s)\tilde{x}_{P0} + G_D(s)\tilde{x}_D] \quad (16)$$

The steady state value $\bar{\tilde{x}}_P$ of \tilde{x}_P is obtained by setting $s = 0$ to give

$$\bar{\tilde{x}}_P = \frac{1}{G_P(0)} [G_{P0}(0)\bar{\tilde{x}}_{P0} + G_D(0)\bar{\tilde{x}}_D] \quad (17)$$

In particular, the steady-state disturbance gain g_D is given by:

$$g_D = \frac{\bar{\tilde{x}}_P}{\bar{\tilde{x}}_D} = \frac{G_D(0)}{G_P(0)} \quad (18)$$

With the parameters given in Figure 3:

$$G_D(0) = 1.00 \quad (19)$$

$$G_P(0) = 4.44 \quad (20)$$

$$\text{hence } g_D = 0.23 \quad (21)$$

This corresponds to Figure 3.

2.4 Split Loop analysis

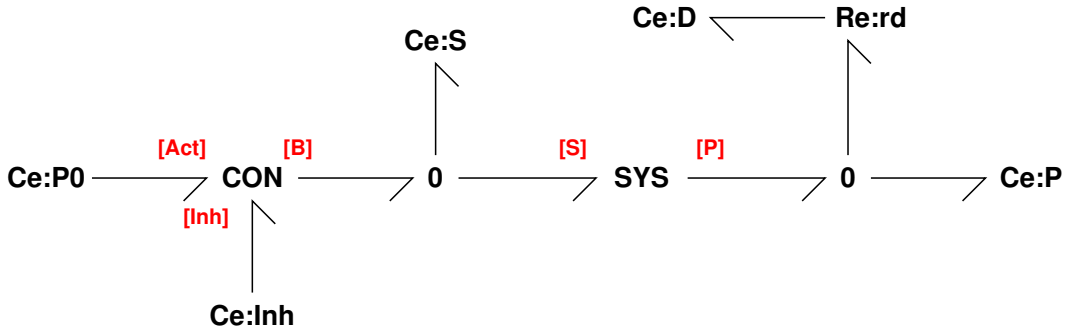


Figure 5: Split-loop. The feedback bond in Figure 2(b) is removed and replaced by the chemostat **Ce:Inh**. This splits the loop and allows active and passive feedback to be distinguished as described in the text.

The previous section shows how the loop gain $L(s)$ may be derived from the closed-loop system in the bond graph form of Figure 2(b). This section expands this analysis by dividing the loop gain $L(s)$ into two parts: an active part $L_{act}(s)$ and a passive part $L_{pas}(s)$ so that

$$L(s) = L_{act}(s) + L_{pas}(s) \quad (22)$$

The active part arises mainly from the properties of the controller (**CON**); the passive part arises mainly from the properties of the system (**SYS**) appearing in the closed-loop bond graph of Figure 2(b).

The *split-loop* procedure is based on removing the feedback bond linking the controlled product **Ce:P** to the inhibition port ([Inh]) of the controller. This is depicted in Figure 5 where the bond has been removed and the chemostat **Ce:Inh** has been added. To focus on the loop gain, the chemostats **Ce:P0** and **Ce:D** are held at the steady state values ($\tilde{x}_D = \tilde{x}_{P0} = 0$) for the rest of this section. The linearised flows \tilde{f}_{PP} into the chemostat **Ce:P** and \tilde{f}_{II} into the chemostat **Ce:Inh** are each given by the sum of two terms corresponding to the two variable chemostats **Ce:Inh** and **Ce:P** respectively:

$$\tilde{f}_{PP} = -G_{PI}(s)\tilde{x}_{Inh} - G_{PP}(s)\tilde{x}_P \quad (23)$$

$$\tilde{f}_{II} = -G_{II}(s)\tilde{x}_{Inh} - G_{IP}(s)\tilde{x}_P \quad (24)$$

When the split-loop is reconnected

$$\tilde{x}_{Inh} = \tilde{x}_P \quad (25)$$

$$\text{and } \tilde{f}_P = \tilde{f}_{PP} + \tilde{f}_{II} \quad (26)$$

$$= -[G_{PI}(s) + G_{PP}(s) + G_{II}(s) + G_{IP}(s)]\tilde{x}_P \quad (27)$$

$G_{PI}(s)$ is the transfer function from the inhibition port of the controller to the product and is thus the active part of the control. Hence the previous equation is rewritten as:

$$\tilde{f}_P = - [G_{act}(s) + G_{pas}(s)] \tilde{x}_P \quad (28)$$

$$\text{where } G_{act}(s) = G_{PI}(s) \quad (29)$$

$$G_{pas}(s) = G_{PP}(s) + G_{II}(s) + G_{IP}(s) \quad (30)$$

Once again, the minus signs associated with G_{act} and G_{pas} are to give compatibility with standard definitions of loop gain in a negative feedback context.

To allow comparison with Equation (13), the transfer functions appearing Equation (23) are evaluated with the *same steady states as those of the closed-loop system* and, in addition, reconnection of the split loop implies

$$\bar{x}_{inh} = \bar{x}_P \quad \tilde{x}_{inh} = \tilde{x}_P \quad (31)$$

Comparing Equations (13 and Equation (23), it follows that:

$$G_P = G_{act} + G_{pas} \quad (32)$$

Further, defining

$$L_{act}(s) = \frac{G_{act}(s)}{s} \quad L_{pas}(s) = \frac{G_{pas}(s)}{s} \quad (33)$$

Equation (22) follows from Equation (32). Thus the block-diagram of Figure 4(a) can be expanded to give the block-diagram of Figure 4(b).

The conventional approach to feedback control in the engineering context would regard L_{pas} as an unwanted artefact to be eliminated by correct design; similarly, in the life-sciences context, L_{pas} would be regarded as due to retroactivity and therefore undesirable [7]. A theme of this paper is that both these attitudes are inappropriate in this context. In the engineering context, using such interactions to improve control are well established as physical-model based control [12–14] In the systems biology context, this paper will show that L_{pas} has a stabilising influence on the control system.

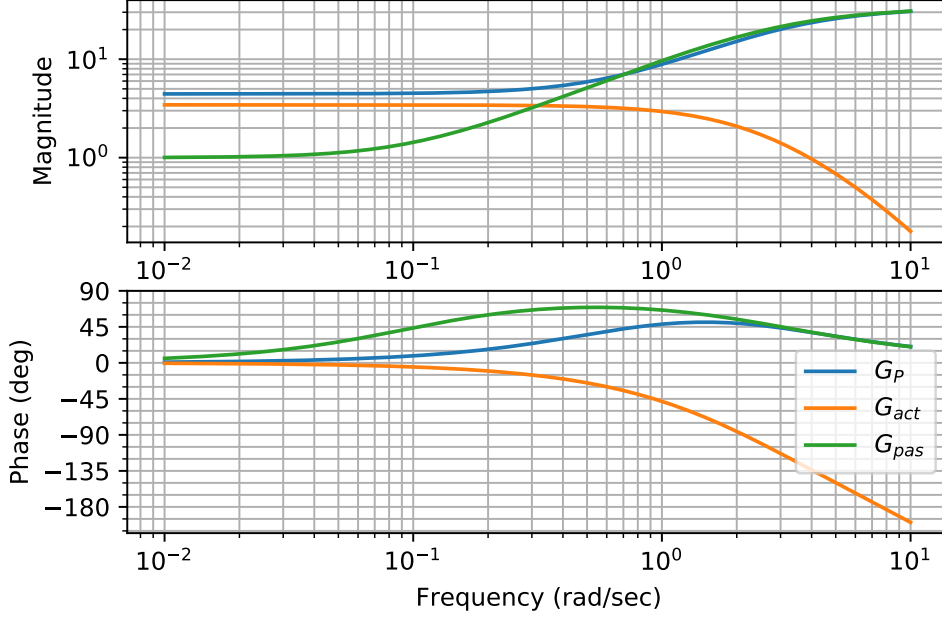
The closed-loop system is given in terms of $G_P(s)$ by Equation (16). Because of the decomposition (32), it is possible to see how the control system would, in principle, behave with only passive or only active control. In particular, if \tilde{x}_{pas} and \tilde{x}_{act} are the product concentration deviations in the two cases:

$$\tilde{x}_{pas} = \frac{1}{s + G_{pas}(s)} [G_{P0}(s)\tilde{x}_{P0} + G_D(s)\tilde{x}_D] \quad (34)$$

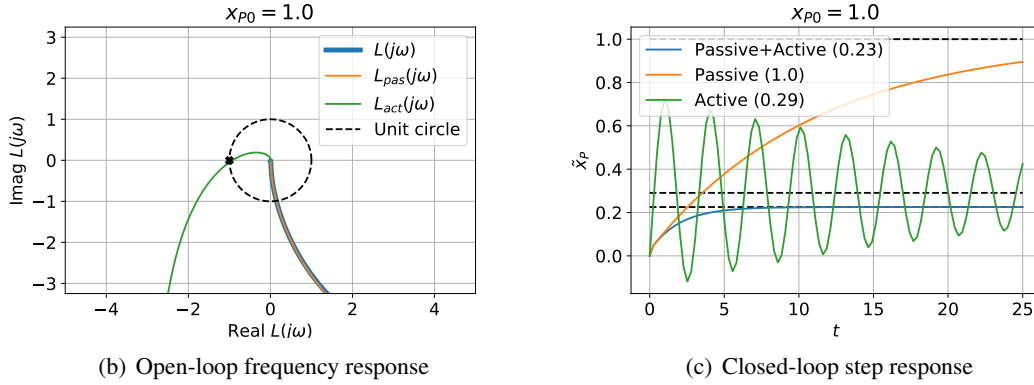
$$\tilde{x}_{act} = \frac{1}{s + G_{act}(s)} [G_{P0}(s)\tilde{x}_{P0} + G_D(s)\tilde{x}_D] \quad (35)$$

Figure 6(a) shows $G_P(j\omega)$, $G_{pas}(j\omega)$ and $G_{act}(j\omega)$ plotted on a Bode diagram [4]. The magnitude of $G_{act}(j\omega)$ is large at low frequencies and small at high frequencies whereas the magnitude of $G_{pas}(j\omega)$ is small at low frequencies and high at high frequencies. Hence the $G_P(j\omega)$ is close to $G_{pas}(j\omega)$ at high frequencies yet retains the high gain at low frequencies due to $G_{act}(j\omega)$.

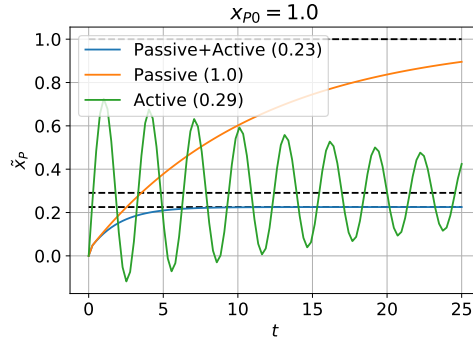
In classical control theory, the *frequency response* of the loop gain reveals dynamical properties – including stability – of the closed-loop system. One such frequency-based approach is based on the



(a) Components of $G_P(s)$



(b) Open-loop frequency response



(c) Closed-loop step response

Figure 6: ECR: Split-loop analysis. (a) Components of $G_P(j\omega)$. $G_{PI} \approx 0$ and is not shown. Of the two remaining components of G_{pas} , G_{II} is small at low frequencies and so $G_{pas} \approx G_{PP}$ at low frequencies; at mid and high frequencies, G_{pas} provides phase advance. G_{act} is large at low frequencies and small at high frequencies. Thus $G_P(j\omega) \approx G_{act}(j\omega) + G_{PP}(j\omega)$ at low frequencies and $G_P(j\omega) \approx G_{pas}(j\omega)$ at high frequency. Thus $G_{act}(j\omega)$ provides high gain (and thus low steady-state error) at low frequencies and $G_{pas}(j\omega)$ provides stabilising phase advance at mid frequencies. (b) Open-loop frequency response. The loop gain $L(j\omega) = \frac{G_P(j\omega)}{s}$ and its two components $L_{act}(j\omega)$ and $L_{pas}(j\omega)$ are plotted on a Nyquist diagram. $L_{act}(j\omega)$ passes close to the -1 point and thus, without the term $L_{pas}(j\omega)$, $L(j\omega)$ would correspond to closed-loop system close to instability. However, at the relevant frequencies, $L(j\omega) \approx L_{pas}(j\omega)$ and is well away from the -1 point and thus corresponds to a stable closed-loop system. (c) Closed-loop disturbance step response. The hypothetical closed-loop responses corresponding to $L_{pas}(j\omega)$ and $L_{act}(j\omega)$ are well damped with large steady-state error and oscillatory with small steady-state error respectively. The actual response corresponding to $L(j\omega)$ combines the best of both.

Nyquist diagram [4] where the imaginary part of $L(j\omega)$ is plotted against the real part of $L(j\omega)$ for a range of frequencies. The phase $\angle L(j\omega)$ when the modulus $|L(j\omega)| = 1$ is of interest, hence the *unit circle* is plotted on the Nyquist diagram of Figure 6(b). There are three frequency responses plotted: $L_{pas}(j\omega)$ shows that, as the frequency response is well away from the -1 point, the time response is well-damped; $L_{act}(j\omega)$ shows that, as the frequency response passes close to the -1 point, the time response is oscillatory; $L(j\omega)$ is similar to $L_{pas}(j\omega)$ near the unit circle and therefore also has a well-damped response.

The corresponding unit step responses appear in Figure 6(c) along with the step response of \tilde{x}_P corresponding to Equation (16). The disturbance response of the passive-only system is well-behaved but the steady-state value is large; in contrast, the disturbance response of the active-only system is oscillatory but the steady-state value is small. The overall controller combines the best of both responses: it is well behaved with a small steady-state value. The numerical steady-state values for the overall controller are given in Equation (21); in a similar fashion:

$$g_{pas} = \frac{1}{G_{pas}(0)} = 1/1.0 = 1 \quad (36)$$

$$g_{act} = \frac{1}{G_{act}(0)} = 1/3.44 = 0.29 \quad (37)$$

Thus the small steady-state value is largely due to the active part of the control.

3 Cyclic flow modulation (CFM)

“The parallel existence of two irreversible reactions is of the greatest importance in metabolic regulation: it means that the direction of flux between two metabolites is determined by differential regulation of the activities of the two enzymes” [18]. A bond graph interpretation of this mechanism appears in Figure 7(a) and this will be used as the basis replacing the **CON** component in the bond graph feedback loop of Figure 2(b) by a more sophisticated control actuator.

The use of such cyclic flow modulators is motivated by the pair of key metabolic reactions discussed by Cornish-Bowden [18]:



This pair of reactions can be related to the CFM bond graph of Figure 7(a) (with reference to Figure 1(b)) as follows. The enzyme corresponding to **ECR:Fwd** is PFK (phosphofruktokinase) and the enzyme corresponding to **ECR:Rev** is FBP (fructose biphosphatase). As noted in Fig. 1, the generic substrate A corresponding to **Ce:A** is replaced by F_6P (fructose-6-phosphate) and the generic product B corresponding to **Ce:B** is $F_{16}P$ (fructose-1,6-biphosphate). Within the module **ECR:Fwd** (see Fig. 1(a)), **Ce:F** corresponds to ATP (Adenosine triphosphate) and **Ce:G** corresponds to ADP (Adenosine diphosphate); within the module **ECR:Rev** (see Fig. 1(a)), **Ce:F** corresponds to H_2O and **Ce:G** corresponds to Pi (inorganic phosphate). This procedure is based on the fact that **Ce** components within a module, that are not exposed as ports, represent a different species for each instance of the module.

Species which activate PFK and inhibit FBP include AMP (Adenosine monophosphate) and $F_{26}P$ (fructose-2,6-phosphate); species which inhibit PFK and activate FBP include ATP and Cit (citrate).

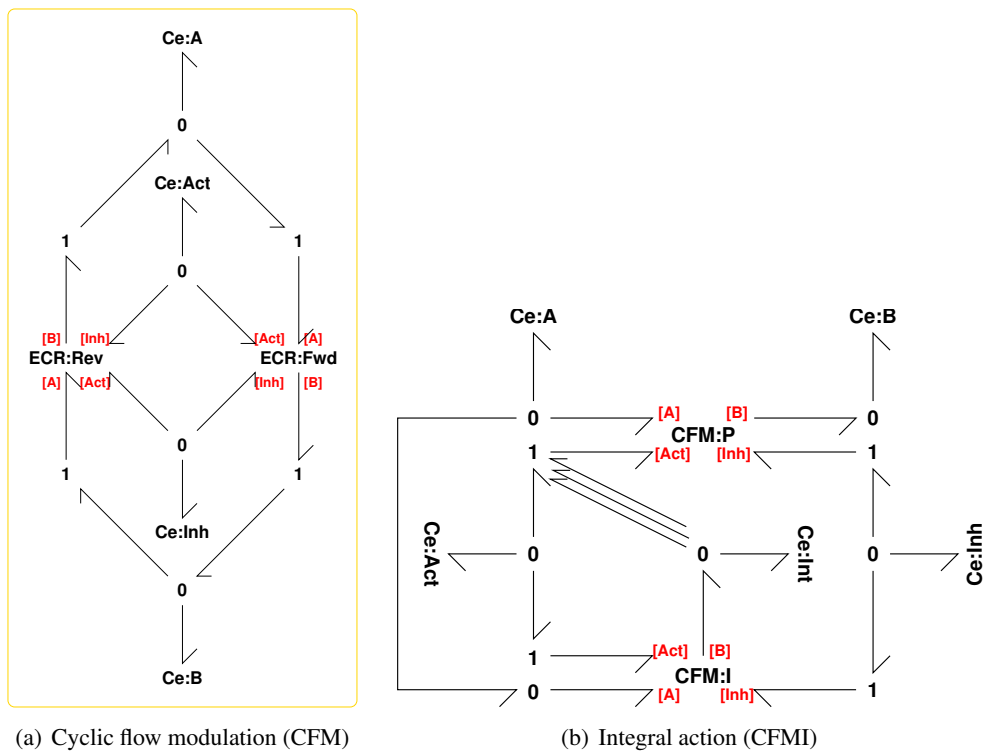
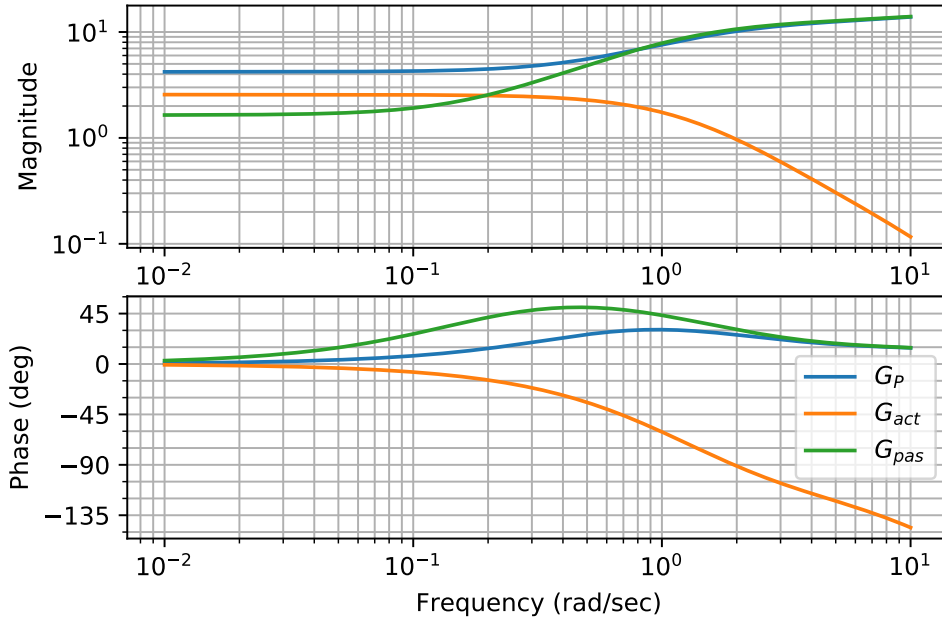
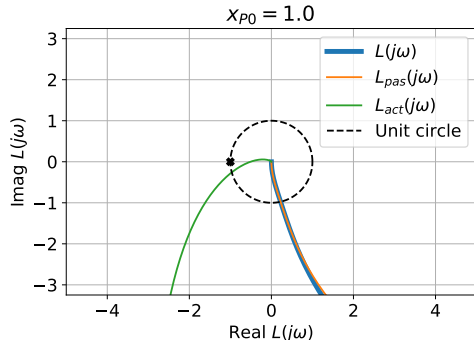


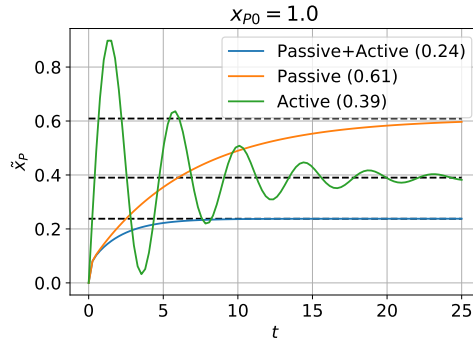
Figure 7: Cyclic flow modulation. (a) The two components **ECR:Fwd** and **ECR:Rev** are instances of the modulated ECR of Figure 1(b). The **Ce:A** component represents both the substrate of **ECR:Fwd** and the product of **ECR:Rev**; the **Ce:B** component represents both the substrate of **ECR:Rev** and the product of **ECR:Fwd**. Component **Ce:Act** both activates **ECR:Fwd** and inhibits **ECR:Rev**; component **Ce:Inh** both inhibits **ECR:Fwd** and activates **ECR:Rev**. (b) **CFM:P** gives proportional (P) action whereas **CFM:I** gives integral (I) action by driving the species **Ce:Inh** which activates **CFM:P**. To exemplify strong activation, three activation bonds are used.



(a) Components of $G_P(s)$



(b) Open-loop frequency response



(c) Closed-loop step response

Figure 8: CFM: Split-loop analysis. The controller **CON** and system **SYS** of Fig. 2(b) are replaced by the CFM module **CFM** of Fig. 7(a) and the pathway module of Fig. 1(c) respectively. Detailed comments and parameters are given in Figure 6; the low frequency gain is higher leading to a lower steady-state error. Once again, the passive term G_{pas} stabilises the high-gain active control term G_{act} .

This section examines the effect of replacing the ECR based control of the feedback loop of Figure 2(b) by a CFM based controller. The ECR module of Figure 1 has four visible chemostats **Ce:A**, **Ce:B**, **Ce:Act**, and **Ce:Inh** the latter three of which are used as ports ([B], [Act], [Inh]) in the feedback loop of Figure 2(b); the same chemostats (**Ce:A**, **Ce:B**, **Ce:Act**, and **Ce:Inh**) are visible in the CFM module of Figure 7(a) and can be used as ports in the same way. Thus the CFM module can directly replace the ECR module in the feedback loop of Figure 2(b) (which was analysed in Figure 6); this CFM-based feedback loop is analysed in Figure 8.

The linearised response of the ECR and CFM are similar for the parameters chosen. However, there is a significant difference: the CFM controller is bidirectional, the ECR is not. In both cases, the constant low-frequency gain corresponds to the *proportional* (P) controller of classical control. In contrast, the next section shows that two CFMs can be combined to give the classical proportional+integral by endowing the controller with *integral action*.

3.1 Integral action

Integral action is an important concept in classical control theory [4] and endows a control system with zero steady-state error. In section 3.5 *Integral feedback in energy metabolism: the forgotten side reaction* of their paper Cloutier and Wellstead [6] discuss the role of F₂₆P (fructose-2,6-biphosphate), a strong activator of PFK (phosphofructokinase). In particular, F₂₆P interconverts with F₆P (fructose-6-phosphate) via the reaction cycle:

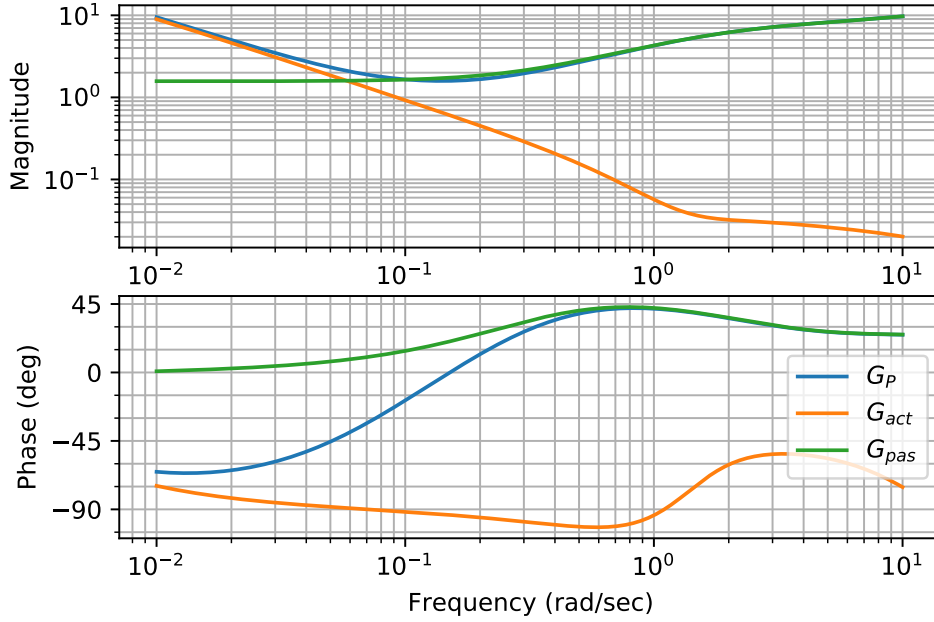


catalysed by the enzymes PFK2 (phosphofructokinase-2) and F₂₆BP (fructose-2,6-biphosphatase). The species which simultaneously activate PFK2 and inhibit F26BP include AMP and F₆P. Hence this pair of reactions is a further example of Cyclic Flow Modulation (CFM).

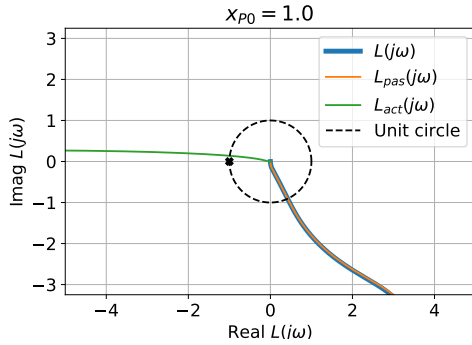
Moreover, the PFK CFM and the PFK2 CFM strongly interact: the PFK CFM is positively modulated by the product of the PFK2 CFM: F₂₆P and both are positively modulated by AMP.

Figure 7(b) gives the bond graph abstraction of the two interacting cycles. **CFM:P** corresponds to the PFK-based CFM giving proportional (P) action whereas **CFM:I** corresponds to the PFK2-based CFM and, as will be seen, gives integral (I) action. Within each CFM, the interpretation of the species is the same except that the product B of **CFM:I** corresponds to F₂₆P rather than F₁₆P. The component **Ce:Int** corresponds to the product F₂₆P which then activates **CFM:P**. For illustration, and to emphasise the strong activation effect, three bonds represent the activation effect.

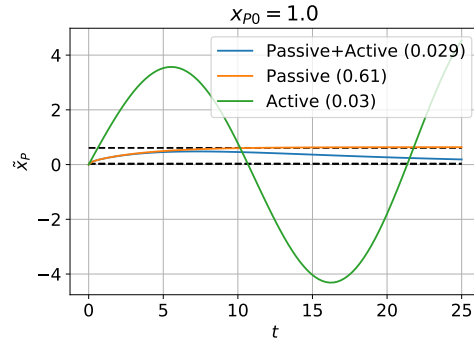
This section examines replacing the CFM based control within the feedback loop of Figure 2(b) by a CFMI based controller. As in the case of CFM, the same chemostats as ECR are visible in the CFMI module of Figure 7(b) and can be used as ports in the same way. Thus the CFMI module can directly replace the ECR module in the feedback loop of Figure 2(b) analysed in Figure 6; this CFMI-based feedback loop is analysed in Figure 9. Compared to the CFM controller response of Figure 8, the low-frequency gain of the active term G_{act} rises as frequency decreases; this is the behaviour expected of an integrator. However, as the integrator is not perfect, the gain is not infinite at $\omega = 0$; but this approximate integral effect gives a significantly lower steady-state error than the CFM controller whilst the passive term G_{pas} continues to act to give a damped response. The disturbance response of the three controllers (using nonlinear simulation) is shown in Figure 10(a); the CFMI controller has a substantially smaller steady-state disturbance error than the other two. For comparison, the



(a) Components of $G_P(s)$

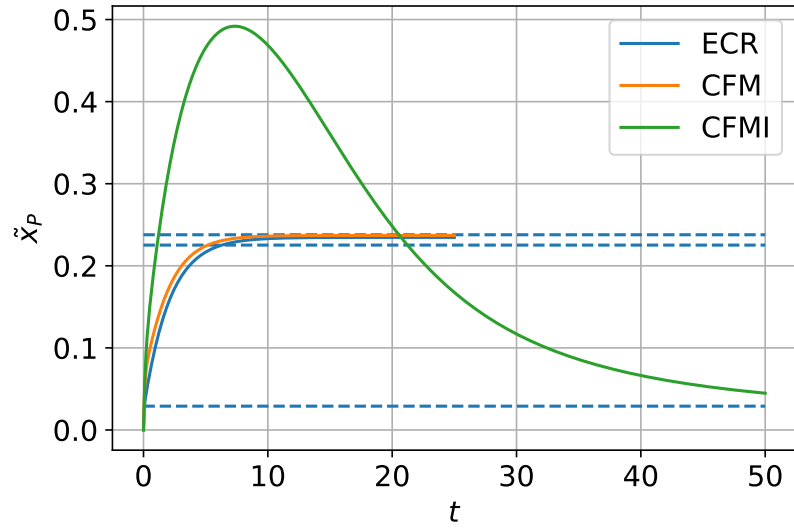


(b) Open-loop frequency response

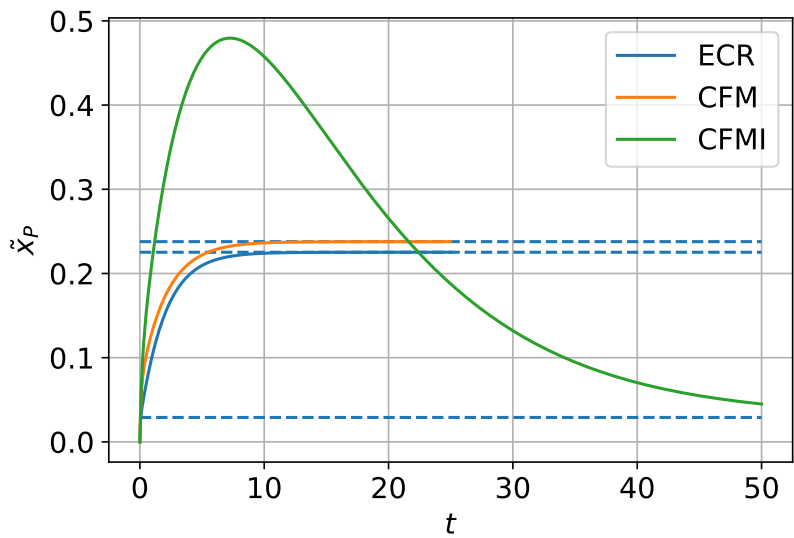


(c) Closed-loop step response

Figure 9: CFMI: Split-loop analysis. The controller **CON** and system **SYS** of Fig. 2(b) are replaced by the CFM module **CFMI** of Fig. 7(b) and the pathway module of Fig. 1(c) respectively. Detailed comments and parameters are given in Figure 6. Compared to the CFM controller response of Figure 8, the low-frequency gain of the active term G_{act} rises as frequency decreases; this is the behaviour expected of an integrator. However, as the integrator is not perfect, the gain is not infinite at $\omega = 0$. This approximate integral effect gives a lower steady-state error than the CFM controller whilst the passive term G_{pas} continues to act to give a damped response. As the phase of $L_{act}(j\omega_c)$ is below -180° at the critical frequency ω_c at which magnitude $|L_{act}(j\omega_c)| = 1$, the closed-loop system corresponding to the active part of the controller is unstable.



(a) Nonlinear



(b) Linearised

Figure 10: Controller comparison. (a) The response of the product concentration deviation from steady-state $\tilde{x}_P = x_P - \bar{x}_P$ to a unit step deviation in disturbance concentration \tilde{x}_D for each of the three controllers ECR, CFM and CFMI is plotted against normalised time t together with the steady state disturbance gains g_D (18) as dashed lines. Thus the CFMI controller is the best of the three in reducing the steady-state error. (b) The linearised responses are shown for comparison; they are close to the nonlinear responses and asymptotically match the disturbance gains g_D (18).

corresponding linearised responses appear in Figure 10(b); they are close to the nonlinear response and, as expected, are asymptotic to the steady state disturbance gains g_D (18).

Performance depends on both controller structure and controller parameters. Figure 10 illustrates that the CFMI structure is superior to both the ECR and CFM structures. As discussed in Figure 1, the generic species F and G provide the energy driving the controller reactions; for example, in reactions (38) and (40), F represents ATP and G represents ADP. Thus the concentrations x_F and x_G together with the parameters K_F and K_G (equation (1)) are crucial to control performance. In particular, the effective controller gain increases with K_F/K_G and the simulated values correspond to the values of K_F and K_G given in Figure 3; thus large K_F/K_G improves controller performance at the expense of increased energy consumption. An analysis of this performance/energy tradeoff is beyond the scope of this paper.

The similarity of linear and nonlinear responses validates the use of linear design approaches in this nonlinear context. It would be interesting to use the frequency response methods of this paper to investigate issues such as robustness to the changes in parameters of the linearised system due to both changes in the equilibria and the parameters of the underlying nonlinear system.

3.2 Steady-state values

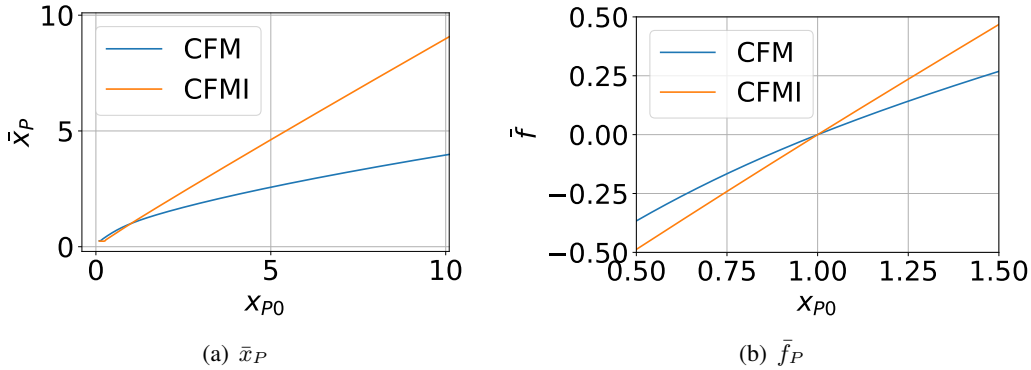


Figure 11: Steady-state. (a) The steady-state product state $\bar{x}_P \approx x_{P0}$ for the CFM and CFMI controllers. (b) The steady-state product flow \bar{f}_P is bidirectional in the case of the two CFM-based controllers; this is not possible for the ECR controller.

In the examples so far, the activation chemostat of Figure 2(b) is defined by a unit state $x_{P0} = 1$. By analogy with the classical feedback loop of Figure 2(a), it would be expected that x_{P0} would play a similar role to w . Figure 11(a) indicates that this is approximately true for the CFMI control: $\bar{x}_P \approx x_{P0}$. Furthermore, varying x_{P0} changes the steady-state product flow. In this case, as the disturbance reaction gain is $\kappa_{rd} = 1$ the product flow $\bar{f}_P = x_P - x_d = x_P - 1$. One of the benefits noted for CFM control at the beginning of § 3 is that bidirectional product flow is possible: Figure 11(b) illustrates this for the CFM and CFMI controller; it is not possible for the ECR controller.

4 Conclusion

Network thermodynamic modelling via bond graphs has been amalgamated with classical control theory. This means that physically-based models of biomolecular systems, which automatically include

features – such as retroactivity – which are not ideal from a control systems viewpoint, can be directly analysed using the transfer function based methods of control theory and the resultant designs are thus biologically feasible. In particular, the dual roles of active and passive feedback have been analysed: active feedback gives good steady state performance whereas passive feedback provides stabilisation.

In this context, cyclic flow modulation (CFM) has been motivated by the phosphofructokinase-fructose biphosphatase cycle of the metabolic pathway and shown to have a modular bond graph representation. The methods of this paper could be used in two ways: to *analyse* the CFM-based control systems arising from evolution and to *synthesise* new cellular control systems. For example, CFM could be used to build biological analogues of the proportional (P) and proportional+integral (PI) controllers of classical control theory, as well as allowing bidirectional flow modulation. Such non-ideal controllers can then be analysed by the methods of this paper and, as models of biological systems, can be directly implemented as biological systems.

Future work will include building an *energy-based* model of metabolism with AMP feedback and mitochondrial transduction using existing energy-based models [26, 31].

An important potential result of combining control theory with energy-based modelling is to identify performance/energy trade-offs and this is the subject of current research. This tradeoff is important to both evolutionary theory [34] and synthetic biology [35].

5 Acknowledgements

Peter Gawthrop would like to thank the Melbourne School of Engineering for its support via a Professorial Fellowship, and Edmund Crampin and Michael Pan for help, advice and encouragement. The suggestions of anonymous reviewers were instrumental in improving this paper.

References

- [1] George Oster, Alan Perelson, and Aharon Katchalsky. Network thermodynamics. *Nature*, 234: 393–399, December 1971. doi:10.1038/234393a0.
- [2] George F. Oster, Alan S. Perelson, and Aharon Katchalsky. Network thermodynamics: dynamic modelling of biophysical systems. *Quarterly Reviews of Biophysics*, 6(01):1–134, 1973. doi:10.1017/S0033583500000081.
- [3] A.S. Perelson. Network thermodynamics. an overview. *Biophysical Journal*, 15(7):667 – 685, 1975. ISSN 0006-3495. doi:10.1016/S0006-3495(75)85847-4.
- [4] Karl Johan Aström and Richard M Murray. *Feedback systems: an introduction for scientists and engineers*. Princeton University Press, 2008. ISBN 978-0-691-13576-2.
- [5] Michael A. Savageau. *Biochemical Systems Analysis. A Study of Function and Design in Molecular Biology*. Addison-Wesley, Reading, Mass., 40th anniversary issue edition, 2009.
- [6] Mathieu Cloutier and Peter Wellstead. The control systems structures of energy metabolism. *Journal of The Royal Society Interface*, 7(45):651–665, 2010. doi:10.1098/rsif.2009.0371.
- [7] Domitilla Del Vecchio, Alexander J. Ninfa, and Eduardo D. Sontag. Modular cell biology: retroactivity and insulation. *Molecular Systems Biology*, 4:1–16, 2008. doi:10.1038/msb4100204.

- [8] Tau-Mu Yi, Yun Huang, Melvin I. Simon, and John Doyle. Robust perfect adaptation in bacterial chemotaxis through integral feedback control. *Proceedings of the National Academy of Sciences*, 97(9):4649–4653, 2000. doi:10.1073/pnas.97.9.4649.
- [9] Yo-Cheng Chang, Judith P Armitage, Antonis Papachristodoulou, and George H Wadhams. A single phosphatase can convert a robust step response into a graded, tunable or adaptive response. *Microbiology*, 159:1276–1285, 2013. doi:10.1099/mic.0.066324-0.
- [10] Dale Muzzey, Carlos A. Gomez-Uribe, Jerome T. Mettetal, and Alexander van Oudenaarden. A systems-level analysis of perfect adaptation in yeast osmoregulation. *Cell*, 138(1):160 – 171, 2009. ISSN 0092-8674. doi:10.1016/j.cell.2009.04.047.
- [11] Yili Qian and Domitilla Del Vecchio. Realizing ‘integral control’ in living cells: how to overcome leaky integration due to dilution? *Journal of The Royal Society Interface*, 15(139):20170902, 2018. doi:10.1098/rsif.2017.0902.
- [12] Dean Karnopp. Bond graphs in control: Physical state variables and observers. *Journal of the Franklin Institute*, 308(3):219 – 234, 1979. ISSN 0016-0032. doi:10.1016/0016-0032(79)90114-5.
- [13] A. Sharon, N. Hogan, and D. E. Hardt. Controller design in the physical domain. *Journal of the Franklin Institute*, 328(5):697–721, 1991.
- [14] P. J. Gawthrop. Physical model-based control: A bond graph approach. *Journal of the Franklin Institute*, 332B(3):285–305, 1995. doi:10.1016/0016-0032(95)00044-5.
- [15] P. J. Gawthrop and E. J. Crampin. Modular bond-graph modelling and analysis of biomolecular systems. *IET Systems Biology*, 10(5):187–201, October 2016. ISSN 1751-8849. doi:10.1049/iet-syb.2015.0083. Available at arXiv:1511.06482.
- [16] E.A. Newsholme, R.A.J. Challiss, and B. Crabtree. Substrate cycles: their role in improving sensitivity in metabolic control. *Trends in Biochemical Sciences*, 9(6):277 – 280, 1984. ISSN 0968-0004. doi:10.1016/0968-0004(84)90165-8.
- [17] H. Qian and D. A. Beard. Metabolic futile cycles and their functions: a systems analysis of energy and control. *IEE Proceedings - Systems Biology*, 153(4):192–200, July 2006. ISSN 1741-2471. doi:10.1049/ip-syb:20050086.
- [18] Athel Cornish-Bowden. *Fundamentals of enzyme kinetics*. Wiley-Blackwell, London, 4th edition, 2013. ISBN 978-3-527-33074-4.
- [19] Reginald H. Garrett and Charles M. Grisham. *Biochemistry*. Cengage Learning, Boston, MA, 6th edition, 2017.
- [20] Guy Shinar and Martin Feinberg. Design principles for robust biochemical reaction networks: What works, what cannot work, and what might almost work. *Mathematical Biosciences*, 231(1):39 – 48, 2011. ISSN 0025-5564. doi:10.1016/j.mbs.2011.02.012.
- [21] Stephanie K. Aoki, Gabriele Lillacci, Ankit Gupta, Armin Baumschlager, David Schweingruber, and Mustafa Khammash. A universal biomolecular integral feedback controller for robust perfect adaptation. *Nature*, 570(7762):533–537, 2019. ISSN 1476-4687. doi:10.1038/s41586-019-1321-1.

- [22] Jinsu Kim and German Enciso. Absolutely robust controllers for chemical reaction networks. *Journal of The Royal Society Interface*, 17(166), 2020. doi:10.1098/rsif.2020.0031.
- [23] Maxwell L. Neal, Michael T. Cooling, Lucian P. Smith, Christopher T. Thompson, Herbert M. Sauro, Brian E. Carlson, Daniel L. Cook, and John H. Gennari. A reappraisal of how to build modular, reusable models of biological systems. *PLoS Comput Biol*, 10(10):e1003849, 10 2014. doi:10.1371/journal.pcbi.1003849.
- [24] Matteo Polettini and Massimiliano Esposito. Irreversible thermodynamics of open chemical networks. I. Emergent cycles and broken conservation laws. *The Journal of Chemical Physics*, 141(2):024117, 2014. doi:10.1063/1.4886396.
- [25] Peter J. Gawthrop and Edmund J. Crampin. Energy-based analysis of biochemical cycles using bond graphs. *Proceedings of the Royal Society A: Mathematical, Physical and Engineering Science*, 470(2171):1–25, 2014. doi:10.1098/rspa.2014.0459. Available at arXiv:1406.2447.
- [26] P. J. Gawthrop. Bond graph modeling of chemiosmotic biomolecular energy transduction. *IEEE Transactions on NanoBioscience*, 16(3):177–188, April 2017. ISSN 1536-1241. doi:10.1109/TNB.2017.2674683. Available at arXiv:1611.04264.
- [27] H. M. Paynter. *Analysis and Design of Engineering Systems*. MIT Press, Cambridge, Mass., 1961.
- [28] Peter J Gawthrop and Geraint P Bevan. Bond-graph modeling: A tutorial introduction for control engineers. *IEEE Control Systems Magazine*, 27(2):24–45, April 2007. doi:10.1109/MCS.2007.338279.
- [29] Peter J. Gawthrop and Michael Pan. Network thermodynamical modeling of bioelectrical systems: A bond graph approach. *Bioelectricity*, 2020. doi:10.1089/bioe.2020.0042. Published Online: 18 Dec 2020.
- [30] James P Keener and James Sneyd. *Mathematical Physiology: I: Cellular Physiology*, volume 1. Springer, New York, 2nd edition, 2009.
- [31] Peter J. Gawthrop, Peter Cudmore, and Edmund J. Crampin. Physically-plausible modelling of biomolecular systems: A simplified, energy-based model of the mitochondrial electron transport chain. *Journal of Theoretical Biology*, 493:110223, 2020. ISSN 0022-5193. doi:10.1016/j.jtbi.2020.110223.
- [32] Peter J. Gawthrop, Joseph Cursons, and Edmund J. Crampin. Hierarchical bond graph modelling of biochemical networks. *Proceedings of the Royal Society A: Mathematical, Physical and Engineering Sciences*, 471(2184):1–23, 2015. ISSN 1364-5021. doi:10.1098/rspa.2015.0642. Available at arXiv:1503.01814.
- [33] P. Gawthrop and E. J. Crampin. Bond graph representation of chemical reaction networks. *IEEE Transactions on NanoBioscience*, 17(4):449–455, October 2018. ISSN 1536-1241. doi:10.1109/TNB.2018.2876391. Available at arXiv:1809.00449.
- [34] Nick Lane. How energy flow shapes cell evolution. *Current Biology*, 30(10):R471 – R476, 2020. ISSN 0960-9822. doi:10.1016/j.cub.2020.03.055.

- [35] Hadrien Delattre, Jing Chen, Matthew J. Wade, and Orkun S. Soyer. Thermodynamic modelling of synthetic communities predicts minimum free energy requirements for sulfate reduction and methanogenesis. *Journal of The Royal Society Interface*, 17(166):20200053, 2020. doi:10.1098/rsif.2020.0053.